Angular Distribution of Secondary Electrons from (100) Faces of Copper and Nickel*†

JAY BURNS
Department of Physics and Chicago Midway Laboratories, The University of Chicago, Chicago, Illinois
(Received February 8, 1960)

The angular distributions of secondary electrons from (001) faces of copper and nickel single crystals have been measured for secondaries in four energy ranges (0–10 ev, 10–20 ev, 20–40 ev, and 40–90 ev) for primary electron energies of 250, 500, and 800 ev. Fine structure was observed which consisted of weak peaks in the angular distribution superimposed on a background having approximately a cosine distribution. After making corrections for the refraction of secondaries at the surface of the crystal, the internal angular distribution peaks fall along principal low-index directions in the crystal as suggested in the quantum-mechanical collision theories of Wooldridge and of Dekker and van der Ziel. The positions, intensities, and widths of the peaks cannot be accounted for in terms of diffraction of the internal secondaries. The observed peaks are believed to be secondaries produced in the initial collision between the primary electron and a lattice electron of the crystal, enough of these secondaries having escaped the crystal without further collisions to make their observation possible. Details of the angular distribution are in agreement with collision theory based on a screened Coulomb interaction with a velocity-dependent screening length. The velocity dependence of the screening coefficient in the screened Coulomb interaction leads to a sharp drop in the inelastic cross section for energy transfers larger than the plasma excitation energy, and it also leads to increased probability for collisions in which the primary suffers only small deflections. The role of the band structure of the crystal in determining the features of the collision is discussed. In Cu and Ni the vacuum level of potential lies in the second Brillouin zone, so only interzone (umklapp) transitions can lead to secondary electron emission from these metals. Surface refraction is treated in terms of a velocity-dependent refractive index, and the experiment offers a means of determining the velocity dependence of the index. Experimental procedures and precautions required to observe the angular distribution fine structure are discussed.

I. INTRODUCTION

FEW measurements[1,2] of the angular distribution of secondary electrons have been reported in the relatively voluminous literature on secondary emission of the past thirty years. The scarcity of information about this important aspect of secondary emission may be ascribed in part to the experimental difficulties inherent in such measurements and in part to the absence of any particularly interesting or noteworthy features in the angular distributions measured to date. As a result most workers in the field have accepted the view, supported by these measurements, that secondary electrons are emitted with very nearly a cosine distribution devoid of any fine structure and that there is little information to be gained by further study of this feature of the emission. The various theories that have been advanced to explain secondary emission have at some point employed approximations and simplifications which lead to the expectation of a cosine angular distribution. Usually the motion of a secondary from the site of its production to the surface of the solid is treated as a diffusion process with a relatively short scattering length, a procedure which randomizes the directions of the secondaries approaching the surface and leads to the prediction of a cosine distribution for the emitted electrons.

Quantum-mechanical treatments of the collision between the primary electron and a lattice electron of the solid have clearly shown[3,4] that the lattice itself can play a role in conserving momentum in the collision. As a result, the newly excited secondary electrons may under certain conditions have their initial momenta oriented generally along the principal axes in the crystal. However, it is only in collisions that excite a lattice electron into a higher Brillouin zone (interzone or umklapp transitions) that the lattice can play a role in conserving momentum; thus the effect can be found most clearly in those solids having the vacuum level of potential in a higher zone than the top of the valence band for in these substances only interzone transitions can yield electrons having enough energy to escape the surface. One more condition must be met in order that the initial orientation of the internal secondaries can be observed, namely that an appreciable fraction of these secondary electrons reach the surface before undergoing a strong scattering collision. This requires a collision mean free path for the secondary electron which is roughly comparable with that of the primary and therefore appreciably larger than values commonly accepted. It must be remembered, however, that these secondary mean free paths are obtained empirically by using the diffusion length as a disposable parameter in an over-all theory to be adjusted finally to produce agreement between measured secondary emission ratios and those predicted by the theory. The diffusion length so de-

* Supported by the U. S. Air Force Office of Scientific Research.
† Thesis submitted in partial fulfillment of requirements for Ph.D. to the Department of Physics, University of Chicago.
[1] H. E. Farnsworth, Phys. Rev. **25**, 41 (1925).
[2] J. L. H. Jonker, Philips Research Repts. **6**, (1951); **8**, 434 (1953); **12**, 249 (1957).
[3] A. J. Dekker and A. van der Ziel, Phys. Rev. **86**, 755 (1952).
[4] D. E. Wooldridge, Phys. Rev. **56**, 562 (1939).

termined contains many of the residual errors introduced along the way by the approximations adopted at various stages in the calculation. It is rather difficult to assess the reliability of mean free paths obtained in this way, and it is not certain *a priori* that the secondary mean free path must be so much smaller than that of the primary as to render the orientation effect of the crystal unobservable.

The possibility that details of the primary collision process might be revealed by secondaries that reach the surface without undergoing further collisions provided the incentive to examine the angular distributions from single crystals more carefully, with special attention given to the preparation of the crystal surface and to the design of the apparatus to minimize the adverse effects of tertiaries and stray electrons scattered from other parts of the tube. The work to be described represents a successful attempt to detect the presence of fine structure in the angular distributions of secondaries from two metals, Ni and Cu, considered to be particularly suitable for such an investigation.

II. THEORY

The sequence of events leading to the emission of secondary electrons from a solid bombarded by primary electrons may be conveniently divided into three processes. First is the initial collision between the primary electron and an electron of the crystal lattice of the solid in which the latter electron gains sufficient energy to be capable of escaping from the crystal. As the internal secondary moves to the surface, it may collide elastically or inelastically with other lattice electrons, and in these collisions it will lose varying amounts of energy and will be deflected from its original path. This process is often treated phenomenologically as a diffusion stage with suitable diffusion and absorption lengths assigned to bring agreement between calculated and observed secondary emission ratios. Finally, as the secondary approaches the surface potential barrier it may be reflected, or it may be refracted and escape from the solid with kinetic energy equal to its kinetic energy within the crystal minus the potential energy of the surface barrier.

Several quantum-mechanical treatments have been given[3–6] for the initial collision between the primary and lattice electrons. The most general of these is due to Dekker and van der Ziel[3]—later amended by van der Ziel[6] who introduced a screened Coulomb interaction to avoid divergences in the original treatment arising from the use of a pure Coulomb interaction. Following the notation of these authors, we consider a collision between a primary electron with wave vector $\mathbf{K}$ and energy $E_p=(\hbar^2K^2/2m)$ and a lattice electron with wave vector $\mathbf{k}$ and energy $E(\mathbf{k})$. Note that in general $E(\mathbf{k})\neq(\hbar^2k^2/2m)$ since the lattice electron is not free, in contrast with the primary which may be regarded as free to a much better approximation. The products of this collision are a scattered primary (wave vector $\mathbf{K}'$ and energy $\hbar^2K'^2/2m$) and an excited lattice electron [$\mathbf{k}'$ and $E(\mathbf{k}')$] which may have enough energy to escape the surface barrier and become an observable secondary electron. It should be remarked that "lattice electron" refers here to any of the electrons of the solid including the tightly bound atomic core electrons. When we refer to valence electrons, we mean electrons whose wave functions are strongly perturbed by the solid binding forces and these include, in addition to the conduction electrons of a metal, the more tightly bound but still not highly localized outer electrons such as the $3d$ electrons in Cu and Ni. Since we shall be concerned with these metals in this paper, we shall take as a model of the solid the simplified, conventional Sommerfeld model shown in Fig. 1. All energies are measured from the bottom of the band except E_s, the kinetic energy of the emitted secondary, which is measured from the vacuum level of potential.

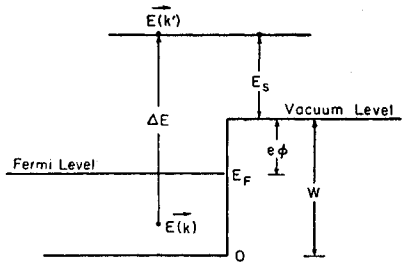

FIG. 1. Sommerfeld model of a metal with notation employed in describing energy relations in inelastic collisions involving excitation of lattice electrons.

Using a one-electron approximation, neglecting exchange and correlation, Dekker and van der Ziel[3] treated the collision by perturbation theory. Van der Ziel's extension[6] to a screened Coulomb potential yielded the following expression for the transition probability

$$P(\mathbf{K},\mathbf{k}\rightarrow\mathbf{K}',\mathbf{k}')d\Omega=\frac{2me^4I^2dqd\phi}{\hbar^2E_pq^3[1+(\lambda^2/q^2)]^2}. \quad (1)$$

In this expression E_p is the initial energy of the primary electron, I is the matrix element

$$I=\int\psi_{\mathbf{k}'}^*(\mathbf{r})e^{i\mathbf{q}\cdot\mathbf{r}}\psi_{\mathbf{k}}(\mathbf{r})d\mathbf{r}, \quad (2)$$

connecting the initial and final states, $\psi_{\mathbf{k}}$ and $\psi_{\mathbf{k}'}$, of the lattice electron. The vector $\mathbf{q}$ is defined by the relation

$$\mathbf{q}=\mathbf{K}-\mathbf{K}', \quad (3)$$

and the quantity λ is the screening parameter in the screened Coulomb potential:

$$V(\mathbf{R}-\mathbf{r})=(e^2/|\mathbf{R}-\mathbf{r}|)e^{-\lambda|\mathbf{R}-\mathbf{r}|}. \quad (4)$$

[5] H. Frohlich, Ann. Physik **13**, 229 (1932).
[6] A. van der Ziel, Phys. Rev. **92**, 35 (1953).

The angle ϕ is the azimuthal coordinate of $\mathbf{K}'$ in a polar coordinate system having its z axis along the wave vector $\mathbf{K}$ of the primary electron. In this system, θ and ϕ define the direction of $\mathbf{K}'$.

Necessary conditions for the nonvanishing of $P(\mathbf{K}, \mathbf{k} \rightarrow \mathbf{K}', \mathbf{k}')$ are

$$\mathbf{k}'=\mathbf{k}+\mathbf{q}+\mathbf{n}$$

and

$$K^2-K'^2=(2m/\hbar^2)[E(\mathbf{k}')-E(\mathbf{k})]. \quad (5)$$

The first of these equations expresses the conservation of momentum and the second the conservation of energy. The vector $\mathbf{n}$ appearing in the momentum equation is a vector of the reciprocal lattice such that $a\mathbf{n}/2\pi$ has integer components where a is the lattice spacing. Transitions for $\mathbf{n}=0$ have $\mathbf{k}$ and $\mathbf{k}'$ in the same Brillouin zone (intrazone transitions) and those for $\mathbf{n}>0$ involve transitions to a higher zone (interzone transitions). Since the vacuum level of potential lies above the first zone in copper and nickel,[7] the interzone transitions are the only ones that can produce secondaries in these metals. This feature makes Cu and Ni well suited for a search for fine structure in the angular distribution, because the smallest nonzero values of $\mathbf{n}$ along the $\langle 100 \rangle$ directions for these fcc metals are 1.74 and 1.79 A^{-1}, respectively, and these values of $\mathbf{n}$ are considerably larger than values of $\mathbf{k}$ and $\mathbf{q}$ for which the transition probability is large. In these metals, therefore, the momentum conservation equation becomes approximately $\mathbf{k}' \approx \mathbf{n}$, showing that the secondaries are initially strongly oriented along the directions of $\mathbf{n}$, that is, along the principal directions in the reciprocal lattice.

In his paper van der Ziel was persuaded by an argument of Marshall[8] that the transition probability for interzone transitions vanished by virtue of the orthogonality of the lattice electron wavefunctions. This argument is valid only for $\mathbf{q}=0$, which actually means no scattering at all since $\mathbf{K}=\mathbf{K}'$ for this case. In all other cases the matrix element I does not in general vanish. That this is so follows from the form that the lattice wave functions must take[9] to satisfy the symmetry conditions of the lattice; that is, they must be sums of Legendre polynomials (Kubic harmonics in the terminology of von der Lage and Bethe) of like parity and between these there exist nonvanishing matrix elements of $e^{i\mathbf{q}\cdot\mathbf{r}}$. The existence of allowed dipole transitions between zones is a well-known example.

A convenient way to represent these interzone transitions is by means of a diagram in reciprocal space in which the collision may be described by the vectors $\mathbf{K}, \mathbf{K}', \mathbf{k}, \mathbf{k}'$. Such a collision diagram is shown in Fig. 2 which, for the sake of simplicity, is drawn for a simple cubic lattice. Extension to the fcc lattice of Ni and Cu is straightforward. In this diagram the primary electron (wave vector $\mathbf{K}$) is considered to be traveling along a [001] direction in the crystal. It collides with a lattice electron of wave vector $\mathbf{k}$. The vector $\mathbf{q}$ resulting from such a collision will lie within the semicircular shaded area on the diagram for the following reasons. First, there exists a minimum value of $\mathbf{q}$ for a given $\Delta E \equiv E(\mathbf{k}')-E(\mathbf{k})$. From Eq. (5) this value is approximately

$$q_{\min} \approx \frac{\Delta E}{\hbar}\left(\frac{m}{2E_p}\right)^{\frac{1}{2}}, \quad (6)$$

where E_p is the initial energy of the primary. Since ΔE must be at least as large as the work function of the metal if electrons excited in a collision are to gain enough energy to excape, $q_{\min}$ will be of the order of 0.05 A^{-1} for the primary energies considered here. On the other hand, inspection of Eq. (1) shows that for $q \gg \lambda$ the transition probability decreases rapidly with q. Thus, the shielding parameter λ imposes a rough cutoff value on q, namely $q_{\max} \approx \lambda$, above which P decreases as q^{-3}, and below which P increases approximately linearly with q (or ΔE).

The shielding parameter λ is commonly considered to be a constant, and for most purposes it may be regarded as such. However, it is well to remember that the shielding we are dealing with is a polarization effect in which a perturbing charge in a crystal causes the surrounding electrons to move in such a manner as to compensate partially for the perturbation, that is, to shield it out. A finite time is required for the readjustment of charge to take place, and until this action reaches equilibrium, the shielding is incomplete. If the perturbing charge is a fast electron moving through the crystal, it may not

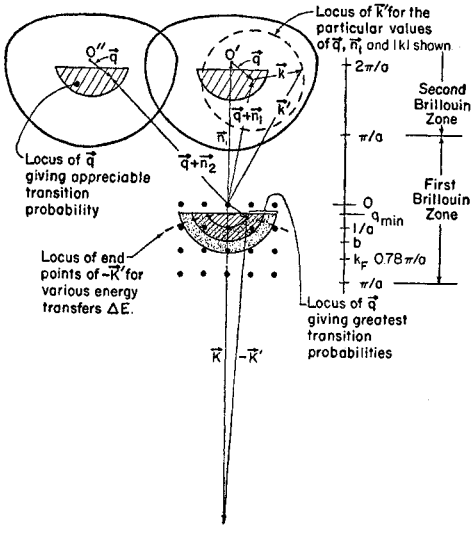

FIG. 2. Diagram in reciprocal space of a collision between a primary electron and a lattice electron resulting in an interzone excitation of the latter. This diagram applies to a simple cubic lattice.

[7] D. J. Howarth, Proc. Roy. Soc. (London) **A220**, 513 (1953).
[8] J. F. Marshall, Phys. Rev. **88**, 416 (1952).
[9] F. von der Lage and H. Bethe, Phys. Rev. **71**, 612 (1947).

remain in any given region long enough for the shielding to approach its static value in that region. We may allow for this by considering the shielding parameter to be a function of the velocity of the primary electron. We do not know the exact velocity dependence of λ but it is reasonable to expect that $\lambda(E_p)$ is a decreasing function of E_p for primary energies greater than some critical value, approaching the static value for primary energies much smaller than the critical energy. The plasma energy $\hbar\omega_p$ would seem to a first approximation to provide a natural division between values of E_p below which λ approaches the static value and above which λ decreases with E_p, since the plasma energy provides a similar separation between collective (lightly screened) and individual particle (strongly screened) interactions in Bohm and Pines' treatment of electron interactions in plasmas.[10] That λ should be proportional to $E_p^{-\frac{1}{2}}$ (i.e., $\lambda \propto v^{-1}$) is suggested by the plasma dispersion relation as well as by the following simple argument. If the characteristic time for electron polarization to reach equilibrium after the onset of a perturbing field is τ, then for times much shorter than τ one would expect that $\lambda/\lambda_0 \approx t/\tau$. A fast primary electron acts as a time-dependent perturbation lasting for a time t inversely proportional to its velocity, leading to the expectation that λ/λ_0 varies approximately as $(\hbar\omega_p/E_p)^{\frac{1}{2}}$ for primary energies much larger than the fundamental plasma energy.

To the extent that λ and q both show the same $E_p^{-\frac{1}{2}}$ dependence on primary energy for $E_p \gg \hbar\omega_p$, the ratio λ/q is independent of primary energy in Eq. (1) for large primary energies and depends only upon ΔE. The result is that there is a cutoff value of $\mathbf{q}$ which corresponds to energy losses ΔE approximately equal to the plasma energy $\hbar\omega_p$, larger losses occurring with rapidly diminishing probability according to Eq. (1). These then are the considerations which lead to the limitations on the size of $\mathbf{q}$ indicated by the shaded areas in Fig. 2. It should be noted also that the upper limit on $\mathbf{q}$ implies that the angle between $\mathbf{K}'$ and $\mathbf{K}$ is small, i.e., that small angle scattering is the dominant process in the collisions under consideration.

Continuing with the discussion of the collision diagram, to $\mathbf{q}$ must be added a reciprocal lattice vector $\mathbf{n}$ which simply transfers the origin 0 to an equivalent point 0′ or 0″. Finally, to the sum $\mathbf{q}+\mathbf{n}$ must be added the initial lattice electron wave vector $\mathbf{k}$. This cannot be determined unambiguously from the information furnished by the experiment, but it can have any direction and any value from zero up to $2\pi/a$ corresponding to the zone boundary. So if at every point $\mathbf{q}+\mathbf{n}$ a circle of radius $k_{\max}$ is drawn, the envelope of all these circles (the somewhat flattened spheroid shown in Fig. 2) delineates the boundary of the end points of all the vectors $\mathbf{k}'=\mathbf{k}+\mathbf{q}+\mathbf{n}$, and every point within one of these spheroids represents a possible $\mathbf{k}'$ vector drawn from 0 to that point. The aggregate of these $\mathbf{k}'$ vectors gives the internal angular distribution of the newly formed secondaries. From this picture it may be seen that the main lobe of the angular distribution along the [001] direction should have a half-width of approximately $\tan^{-1}(\frac{1}{2})=27°$ while the lobes along higher index directions should be sharper. It may also be seen that the angle of incidence of the primaries should have only a very minor influence on the angular distribution.

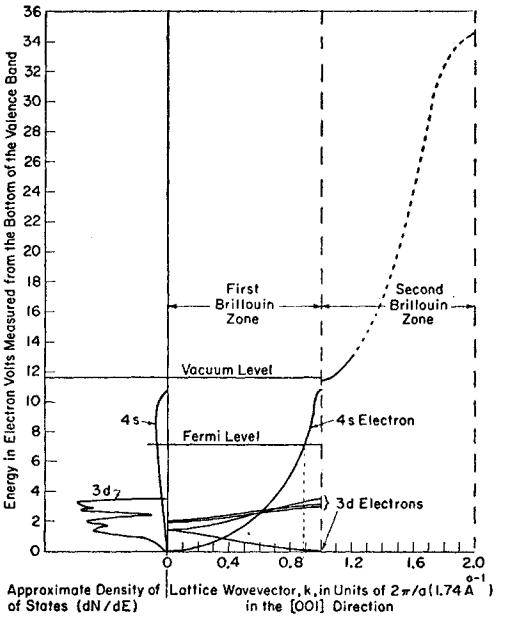

FIG. 3. $E(\mathbf{k})$ curve for copper along the [001] direction (after Howarth) and density of states function for fcc metals (after Koster).

The energy band structure of the metal influences the angular distribution of secondaries through the relation between E and $\mathbf{k}$, through the matrix element I, and through the density-of-states function. In Dekker and van der Ziel's treatment the weighting effect of the density of states was not considered, and since no application to a particular metal was made, the role of the $E(\mathbf{k})$ function was not considered in detail. In Fig. 3 the $E(\mathbf{k})$ versus $\mathbf{k}$ curve along the [001] direction in k space is shown for copper[7] together with the approximate density of states curve for a fcc crystal.[11] The extension of $E(\mathbf{k})$ into the second Brillouin zone is merely schematic, since the band structure has not been determined for these states. Making use of the inverse proportionality between the density of states and $\nabla_{\mathbf{k}}[E(\mathbf{k})]$ one expects large densities of states near the boundaries of this second zone. Combining the work function of Cu($e\varphi \cong 4.50$ ev) with the energy of the Fermi level (7.1 ev), the vacuum level should lie approximately 11.6 ev above the bottom of the valence band which places it definitely beyond the first Brillouin zone.

[10] D. Bohm and D. Pines, Phys. Rev. **82**, 625 (1951); **85**, 338 (1952); **92**, 609 (1953); D. Pines, Phys. Rev. **92**, 626 (1954).

[11] G. F. Koster, Phys. Rev. **98**, 901 (1955); J. C. Slater, Phys. Rev. **49**, 537 (1936).

Whether it falls in the second zone or on the forbidden gap along this [001] direction is not certain at present, although if it fell in the gap, this would give rise to anomalies in other electron emission phenomena from the (100) face (e.g., thermionic, photoelectric) which have not been reported.

The maxima in the densities of the $3d$ electrons in Cu and Ni are for two groups of electrons, one with $k\approx 0$, the other with $k\approx 2\pi/a$. The first group should give rise to a relatively sharp series of lobes in the angular distribution while the second group is responsible for the much broader lobes discussed earlier in connection with Fig. 2. In the present experiment there was some evidence that the [011] lobes were narrow enough to have originated with $k\approx 0$ group of electrons; however, due to experimental limitations it was difficult to determine the detailed shape of the [011] lobe with any certainty. The other lobes appeared broad enough to be accounted for mainly by the $k\approx 2\pi/a$ group of electrons, although it is not possible to say definitely that the other group did not make some contribution.

The internal secondary electrons have their angular distribution strongly distorted by refraction and total internal reflection at the surface of the metal. The simple Sommerfeld model of a metal (Fig. 1) regards the electrons inside as moving in a uniform internal potential W. An electron moving toward the surface inside the metal at an angle θ' from the surface normal is refracted and appears outside at θ with the kinetic energy E_s. From the usual law of refraction

$$\frac{\sin\theta}{\sin\theta'}=\left[1+\frac{W}{E_s}\right]^{\frac{1}{2}}. \tag{7}$$

This picture is too simple for our purposes. A secondary electron inside the crystal with wave vector $\mathbf{k}'$ has a velocity $\mathbf{v}(\mathbf{k}')=(1/\hbar)\nabla_{\mathbf{k}'}E(\mathbf{k}')$ and the more general law of refraction becomes

$$\frac{\sin\theta}{\sin\theta'}=\frac{\nabla_{\mathbf{k}'}E(\mathbf{k}')}{\hbar(2eE_s/m)^{\frac{1}{2}}}. \tag{8}$$

We should expect the index of refraction, $\sin\theta/\sin\theta'$, to depend upon $\mathbf{k}'$ as well as upon E_s if the secondaries inside the metal may not be regarded as free electrons. In general, the refractive index would be anisotropic, depending on the direction of $\mathbf{k}'$ as well as its magnitude. In the present work it has been necessary to use different values of the refractive index for different energy groups of secondaries in order to obtain consistent angular distributions. The assumption that the index is isotropic was adequate to account for the results within the limits of accuracy of the present experimental data, although more precise measurements might reveal the expected directional dependence of the index.

It should be pointed out that the $\mathbf{k}'$ dependence of refractive index here follows Eq. (8) rather than (7) and therefore would seem to support Slater's views[12] about the inadequacy of the free-electron approximation for these excited states. However, the refractive index values determined in this work are averages over relatively large ranges of secondary electron energies and therefore are not sufficient to determine the $E(\mathbf{k})$ curves and the departure from free electron states in the second and higher zones by working backward from Eq. (8), as might be done in principle.

Surface refraction also alters the measured angular distribution through its effect on the element of solid angle $d\Omega$. Jonker[13] has discussed this point and has shown that only a cosine distribution is unchanged by this effect. Consequently, it was necessary to correct all of the observed angular distributions, first for solid angle, then for ordinary refraction, to obtain the angular distributions as they would appear inside the crystal. It is these latter curves which are discussed presently in terms of the scattering process described in the foregoing.

The quantity which is measured experimentally is the secondary electron current emitted into the incremental solid angle $d\Omega$ subtended by the electron collector. If $J(\theta,\phi)$ is the secondary current per unit solid angle emitted in the direction (θ,ϕ), then the collector current in this direction is $J(\theta,\phi)d\Omega$. These same electrons travel in direction (θ',ϕ) inside the metal where $\theta'=\arcsin((v/v')\sin\theta)$ and v',v are the velocities inside and outside the metal respectively. If the current density inside the metal is $J(\theta',\phi)$, then $J(\theta',\phi)d\Omega'$ is the current that the electron collector would measure inside the metal corresponding to the current $J(\theta,\phi)d\Omega$ outside. The ratio $J(\theta,\phi)/J(\theta',\phi)$ is therefore the ratio $d\Omega'/d\Omega$ of the incremental solid angles and this quantity is

$$\frac{J(\theta',\phi)}{J(\theta,\phi)}=\frac{d\Omega}{d\Omega'}=\frac{\eta}{\cos\theta}(\eta^2-\sin^2\theta)^{\frac{1}{2}},$$

where the index of refraction η is given by the expression

$$\eta=\frac{v'}{v}=\frac{\nabla_{\mathbf{k}'}E(\mathbf{k}')}{\hbar(2eE_s/m)^{\frac{1}{2}}}.$$

The internal angular distribution $J(\theta')$ is obtained from the measured external distribution by applying first the solid angle correction above and then refraction correction, $\theta'=\arcsin((1/\eta)\sin\theta)$. Note that the dependence of the above current density ratio on azimuth angle ϕ is contained implicitly in η since the refractive index is proportional to $\nabla_{\mathbf{k}'}E(\mathbf{k}')$, and in general this velocity $\mathbf{v}'$ will not be independent of direction. In the present experiment the refractive index could not be determined with great enough precision to detect any angular dependence of η.

[12] J. C. Slater, Revs. Modern Phys. **30**, 197 (1958).
[13] J. H. L. Jonker, Philips Research Repts. **12**, 249 (1957); **8**, 434 (1953).

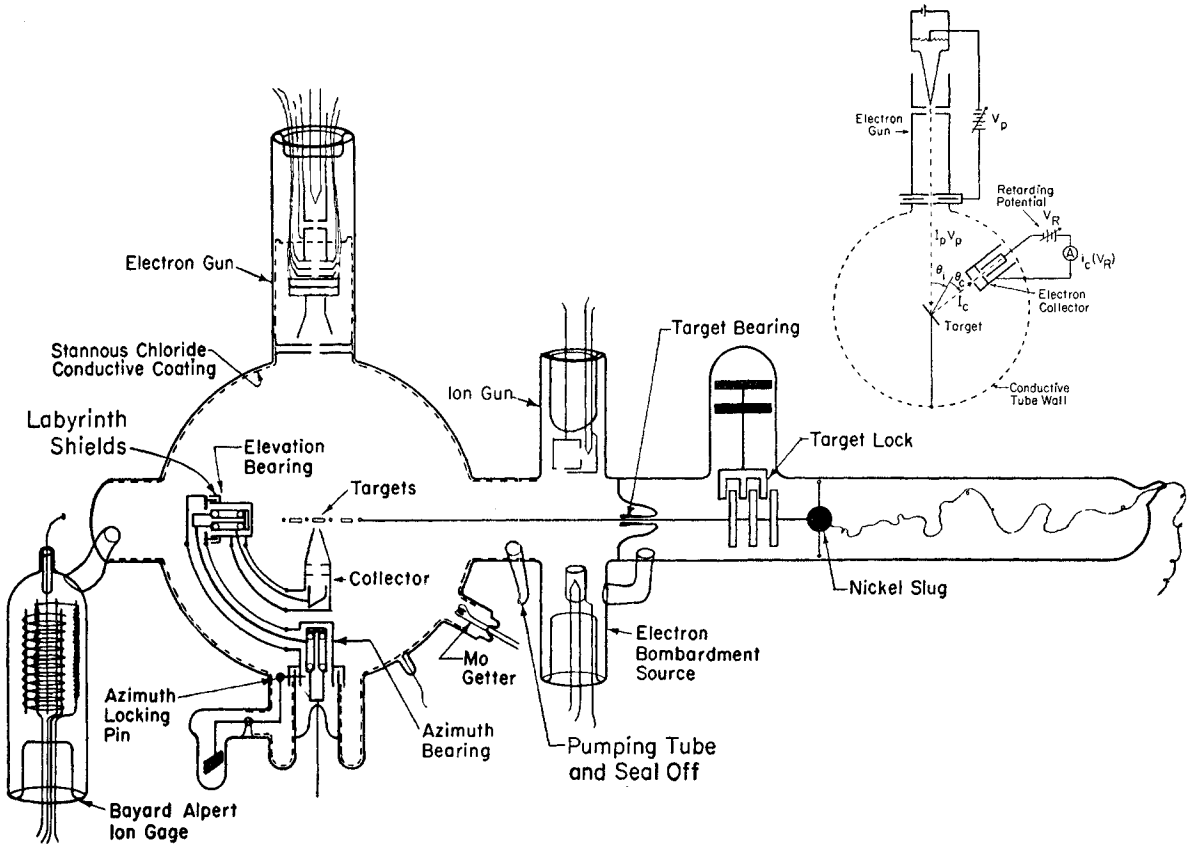

FIG. 4. Secondary emission angular distribution apparatus.

III. EXPERIMENTAL

There are three principal requirements of an apparatus for accurate angular distribution measurements. First, the secondary electrons from the target must be emitted into a sensibly field-free region so they travel in straight paths from the point of emission at the target to the entrance of the electron collector. Second, care must be taken to reduce the effects of stray electrons in the tube. Finally, the target surface must have a well-defined and reproducible physical state. The last requirement is clearly essential to any measurement of secondary emission which is to be interpreted in terms of fundamental processes, and it is here interpreted to mean that the target should be a smooth, strain-free, atomically clean face of a pure single crystal.

The apparatus used is shown in schematic form in Fig. 4 with the circuit shown in the inset. It consists of an electron gun to focus the primary electron beam on the target, together with a movable electron collector to measure the secondary electron current as a function of angle. Provision is made to observe secondaries within selected energy ranges by means of retarding potentials applied to the Faraday cage in the collector. The axes of the two bearings which support the collector assembly intersect the primary beam at the surface of the target, and a combination of rotations about the two bearing axes makes it possible to scan virtually the full hemisphere into which secondaries are emitted except for a small region near the primary beam where the beam is intercepted by the collector. This excluded region extends approximately 8° on either side of the beam. In operation the azimuth bearing is locked by means of a pin which can be inserted and withdrawn magnetically, and the other bearing is left free to rotate. The tube is positioned so the collector hangs vertically under its own weight, and the tube itself is rotated so the freely hanging collector scans the secondary emission current in a longitudinal plane as a function of the co-latitude angle θ. The retarding potential method employed to select ranges of secondary energies for measurements requires that moderately large potentials be applied to the inner conductor and Faraday cage of the collector. These potentials must be carefully shielded if the region between target and collector is to remain field-free.

Equally important, there are stray electron currents in the tube which come from reflected and tertiary electrons produced at the walls of the tube under bombardment by secondaries from the target, and these must be prevented from entering the collector or from striking the inner conductor at the bearings. For this

reason the coaxial labyrinth shields shown in Fig. 4 were used to surround the bearings, and a long conical snoot was used at the entrance to the collector to prevent stray electrons from entering there. Even though the tube was large (a 5-liter flask was used) and the walls were coated with a material (Mo) of relatively low secondary emission ratio, the stray electron density was large enough to mask completely the fine structure in the angular distribution in early versions of the tube when either the snoot or the shields were omitted. This experience suggests one possible reason why fine structure in the angular distribution has not been observed previously.

In regard to maintaining a field-free region within the tube, a simple calculation shows that if such fields are not to cause a measurable error in the angular distribution of the slowest secondaries of interest when the collector subtends an angle of 4° at the target, the magnetic fields (earth's field, residual fields of the nickel slugs used to operate parts of the tube magnetically, ac magnetic fields in the vicinity of the apparatus, etc.) must be reduced to a few milligauss, and the electric fields (chiefly due to contact potential variations inside the tube) must be reduced to a few millivolts per centimeter. In this experiment the earth's magnetic field was compensated by a pair of 2-meter Helmholz coils operated from storage batteries, and the residual field over the region of the tube did not exceed 3 milligauss, according to tests made by measuring the deflection of a low energy electron beam, the figure 3 milligauss being the limit of sensitivity of the test method. Likewise the ac fields were below this limit as were also the residual fields of the nickel slugs after they were demagnetized by means of an ac degaussing coil. Electric fields were shielded out of the tube by application of a grounded conductive layer of stannous chloride[14] to the inside walls of the glass envelopes and a conductive layer of platinum (Hanovia No. 130-A) to the outside of the glass parts of the collector assembly. Finally, contact potentials were equalized as fully as possible by evaporating a layer of molybdenum a few monolayers thick onto the inside walls of the tube and onto the collector and its supporting structure just before making a series of measurements. The targets were protected in a side tube during the evaporation from a Mo filament located inside the tube as shown. During the final stages of evacuation of the tube, and after seal-off, freshly evaporated layers of Mo also served as effective getters for cleaning up the residual adsorbable gases in the tube.

The electron gun was an RCA type B gun modified by substituting a tungsten hairpin filament for the usual oxide cathode and enlarging the grid aperture to 0.060-in. diameter to provide better focusing and grid control. Two shields were added between the last deflection plates and the main target chamber of the tube to ensure that neither electric fields nor stray electrons from the gun could enter the target region.

Provision was made to draw the targets into a sidearm as shown in Fig. 4 by means of a nickel slug attached to the sliding rod which carries the targets. In the sidearm the targets could be cleaned by ion bombardment and annealed and degassed by electron bombardment. In this position the target faces were also protected against contamination by Mo when the Mo getter film was evaporated onto the tube walls prior to a run. The targets were positioned at the center of the tube by means of a simple magnetically operated indexing mechanism (Fig. 4) consisting of a series of fins attached to the target support rod, the desired fin being engaged by a magnetically operated claw which prevented further sliding motion of the fin but allowed the fin and target to be rotated to change the angle between the target normal and the incident electron beam. In this way the angle of incidence of the primary beam could be varied in the plane perpendicular to the target support rod. A magnetically operated sliding latch served to lock this mechanism so it would not disengage when the tube was rotated as the measurements were made. A similar latch was also used on the azimuth locking pin which serves to fix the azimuthal plane of rotation of the collector.

The collector current was measured with a Keithley Model 410 micromicroammeter. This instrument was carefully insulated from ground, and the retarding potentials were applied by varying the potential of the entire electrometer, case and all, with respect to ground. The retarding voltages were obtained from a precision 10-turn potentiometer connected across a battery stack. The output from the electrometer amplifier was fed into a Varian recorder mounted over a turntable to provide a polar coordinate plot of collector current vs collector angle, and the polar chart drive was synchronized with the motor driven frame which rotated the sealed-off tube to vary the angle the collector makes with the target crystal face, as described earlier. The data obtained in this way consisted of a series of polar curves of secondary electron current entering the collector against the retarding potential as a function of collector angle, a separate curve being plotted for each value of retarding potential. The radial differences between any two such curves give the angular distribution of the secondaries in the energy increment represented by the retarding potential differences between the curves.

The pumping system consisted of a three-stage, water-cooled, fractionating, all-glass, oil diffusion pump backed by a mechanical forepump with a liquid nitrogen trap between to prevent contamination of the diffusion pump oil by the forepump oil. On the high vacuum side two liquid nitrogen, copper foil traps were used in series. The first of these was located below the bakeout oven where it could be baked out separately by means of flexible heating tapes. The second was located inside the bakeout oven. After its initial bakeout, the lower trap

[14] R. Gomer, Rev. Sci. Instr. **24**, 993 (1953).

was kept filled with liquid nitrogen by means of an automatic filling device for the duration of the evacuation schedule. Between the upper trap and the tube, a magnetically operated ball joint valve was placed. The purpose of this valve was to isolate the tube from the pump while argon was admitted for ion bombardment cleaning[15] of the target crystals.

The gas handling system for admitting the argon consisted of a Bills and Allen valve[16] between the experimental tube and a one-liter flask, all inside the bakeout oven, followed by another valve and a flask of spectroscopically pure argon outside the oven. The intermediate flask contained an ionization gauge and a molybdenum getter filament whose purpose was to purify the argon further before it was admitted to the tube.

The targets were prepared from single crystal specimens of spectroscopic purity (total impurity content $\lesssim 10$ ppm) from two sources. The nickel crystal was obtained from the Virginia Institute for Scientific Research, 326 North Boulevard, Richmond, Virginia, and the copper crystal was grown at the Institute for the Study of Metals, University of Chicago. The crystals were oriented by x rays (Laue back reflection method) and by etching. The etchant for Cu was a saturated solution of ferric chloride in 25% hydrochloric acid. This etch used at room temperature develops the {100} planes most readily. The Ni crystals were etched in 55% HNO_3 when a rapid etch was desired, followed by the same $FeCl_3$+HCl etch used on Cu. The latter etch works more slowly but develops the crystal faces more clearly without the pitting produced by HNO_3.

The etched crystals were mounted in a goniometer and orientation was carried out by observing the positions at which the crystal facets flashed out reflecting a collimated light beam. The orientation could be checked by x-ray diffraction without removing the crystal from the goniometer. With care the two methods agreed within about 0.5°.

The nickel crystal was cut with a very fine jeweler's saw. The saw marks were removed with metallographic polishing paper followed by a series of alternate ferric chloride etches and electropolishes in 50% H_3PO_4. With care it was possible to remove a thickness of as much as $\frac{1}{2}$ mm from the (100) face maintaining a flat, well-oriented surface which was mirror smooth after the final electropolishing treatment and which contained a very few pits (estimated pitted area $<2\%$). The reason for removing such a large amount of material was to ensure complete removal of the surface layer damaged in cutting and polishing, the objective being a strain-free surface. Laue photographs of the crystal after cutting and polishing but before etching and electropolishing showed diffraction spots with considerable distortion. The final surface, however, gave sharp, symmetrical Laue spots indicating that the disturbed layer had been removed.

Surface damage penetrates much deeper into a Cu crystal than into Ni so a different method of cutting the crystal was employed. Following a technique described by Maddin and Asher,[17] the crystal was cut by a Saran multifilament thread wet with 55% HNO_3. The resulting (100) face gave sharp Laue spots without further treatment. However, to produce a face which was mirror smooth and flat, the alternate etching and electropolishing cycle was employed just as in the preparation of the Ni crystal, using the same reagents. Both crystals were washed thoroughly in triple distilled water, distilled acetone, and methyl alcohol and dried rapidly. They were stored in a vacuum dessiccator prior to being mounted in the experimental tube.

The crystals were supported by threads made from four 0.001-in. diam tungsten wires twisted together and passed through 0.020-in. holes drilled near the periphery of the $\frac{3}{8}$-in. diam crystals. These threads were drawn tight and spot welded to the Mo wire frame on which all targets were supported. This method of mounting was rigid enough for this work, and it provided a means for heating the targets by electron bombardment with a minimum of contamination from the support and with minimum conductive heat loss (approximately 90% of the heat loss was by radiation).

The vacuum processing was straightforward. The tube (minus the targets) was evacuated and baked (together with the upper trap and the gas handling system) for several days at 450°C until the pressure at the entrance to the oven just above the first trap fell below 5×10^{-7} mm Hg with the system hot. Then the tube was cooled and all accessible parts were degassed by induction heating, all filaments were operated, and some parts of the tube were heated by electron bombardment. This was followed by more baking and again by degassing of the metal parts and so on until further induction heating did not evolve any significant amount of gas. Then the upper trap was filled with liquid nitrogen, and the Mo getter was flashed briefly. This reduced the pressure to below 1×10^{-9} mm Hg as read on one of the two Westinghouse WL-5966 ionization gages (Bayard-Alpert type) attached permanently to the tube itself. If the vacuum remained below 10^{-9} mm Hg after closing the glass valve between the tube and the pump, the tube was considered ready for the targets. It was then opened, the targets inserted, and the evacuation schedule repeated. A good vacuum could be obtained rapidly this time, and when it was possible to maintain a vacuum better than 10^{-9} mm Hg with the valve to the pump closed after thoroughly degassing the targets by electron bombardment (to 950°C for Cu and 1300°C for Ni as measured by an optical pyrometer), then pure argon was admitted to a pressure of 1–10 microns, and the faces of the targets were bombarded with 400-ev argon ions (100 μa) for

[15] H. E. Farnsworth, R. E. Schlier, T. H. George, and R. M. Burger, J. Appl. Phys. **26**, 252 (1955).
[16] D. G. Bills and F. G. Allen, Rev. Sci. Instr. **26**, 654 (1955).
[17] R. Maddin and W. R. Asher, Rev. Sci. Instr. **21**, 881 (1950).

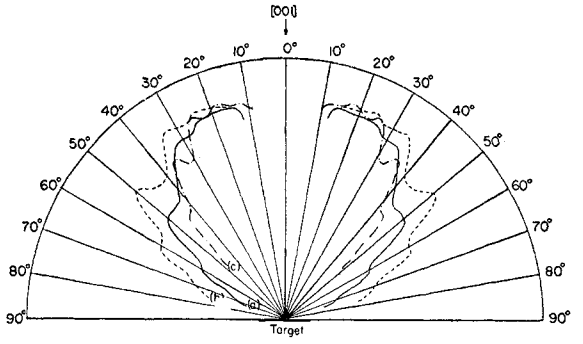

FIG. 5. Copper crystal, (001) face, 250-volt primary beam at normal incidence. All curves are for 0–10 ev secondaries showing (a) data uncorrected for solid angle or refraction; (b) data corrected for solid angle; (c) final curve corrected for solid angle and refraction using index of refraction 1.29.

a period of about 15 minutes after which the argon was pumped out and the crystals were annealed at 600–700°C.

This procedure was repeated three or four times. When the argon had been completely pumped away, a final check on the vacuum was made by closing the valve to the pump, flashing the getter filament and pumping with the ionization gauge for a few hours. The total pressure at this point was usually about 5×10^{-10} mm Hg (in one case 2×10^{-10} mm Hg). With care the seal-off could be accomplished without raising the pressure above 2×10^{-9} mm Hg. Evaporating a little Mo and ion pumping a few hours yielded pressures of about 5×10^{-10} mm Hg again, and this was the minimum total pressure after seal-off. As atmospheric helium diffused into the tube through the walls, the total pressure rose to about 2 to 5×10^{-9} mm Hg where it reached equilibrium with the ionization gauge pumping rate in about two weeks.

Periodic evaporation of a little Mo progressively reduced the partial pressure of adsorbable gases until after about two weeks monolayer formation times were obtained that ranged from a few weeks to approximately

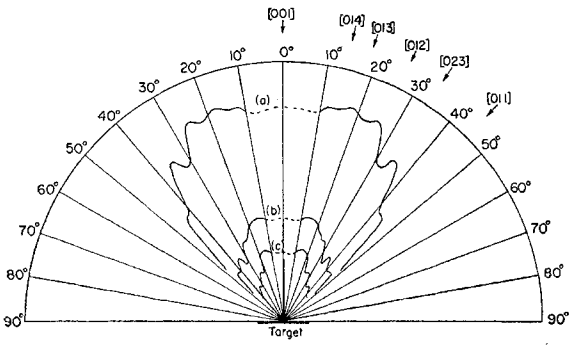

FIG. 6. Copper crystal, (001) face, 250-volt primary beam at normal incidence. Curve (a) is for 0–10 ev secondaries; index of refraction 1.29. Curve (b) is for 10–20 ev secondaries; index of refraction 1.36. Curve (c) is for 20–40 ev secondaries; index of refraction 1.48.

one year, which was the limit sensitivity of the flash-filament technique used to measure the adsorption time. During the period in which the vacuum was improving, the electron gun was operated frequently for prolonged periods and the targets were heated to 800°C occasionally. Eventually, none of these operations produced any observable rise in pressure in the tube (i.e., $<10^{-10}$ mm Hg). Actual measurements were not begun until the monolayer formation time exceeded a month (partial pressure of adsorbable gases $<3\times10^{-13}$ mm Hg, assuming a sticking probability of unity), ensuring that a run could be completed before more than a few percent of the target surface was contaminated by adsorbed gas.

The flash-filament technique was used in the following manner. Earlier in the processing schedule when the partial pressure of adsorbable gases was high enough (10^{-8} to 10^{-9} mm Hg) to give a monolayer in a reasonable time, the flash filament was calibrated in the usual way by measuring the momentary pressure rise in the system when the filament was heated rapidly as a func-

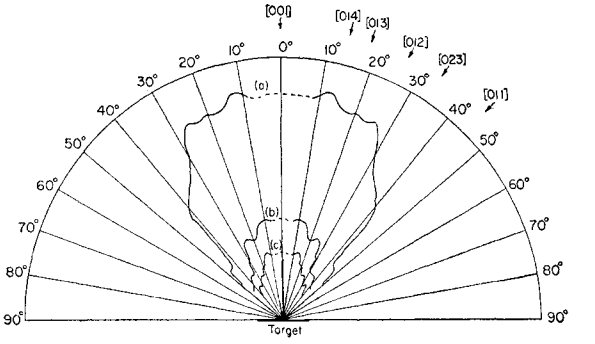

FIG. 7. Copper crystal, (001) face, 500-volt primary electron beam, normal incidence. Curve (a) is for 0–10 ev secondaries, index of refraction 1.29. Curve (b) is for 10–20 ev secondaries, index of refraction 1.36. Curve (c) is for 20–40 ev secondaries, index of refraction 1.48.

tion of the elapsed time since the preceding flash. In this way the pressure rise could be determined as a function of the partial coverage of the filament. Then when the vacuum improved, the monolayer formation time could be found by extrapolating the time required to produce partial coverage of the filament. With care partial coverages as low as 0.1% could be measured corresponding to pressure rises of 10^{-10} mm Hg upon flashing the filament.

The measurements were made in the manner outlined earlier. The sealed-off tube was mounted in a motor driven cradle which rotated it in such a way that the electron collector, hanging free under its own weight, moved slowly from $\theta=+90°$ to $\theta=-90°$ with respect to the target normal. The azimuthal plane in which the collector moved could be varied in ten-degree increments. The target could be rotated to vary the angle of incidence of the primary beam from normal to near-grazing, the limit being set principally by the diameter

(~0.7 mm) of the electron beam. As the collector traced out its path, the electron current into the Faraday cage was recorded as a function of angle θ, and a separate run was made for each retarding potential applied to the Faraday cage. A series of such runs was made for each combination of primary beam energy and angle of incidence.

The lower limit on primary beam energy was approximately 200 ev. Below 200 volts the current from the electron gun was too small for accurate measurements. The upper limit was approximately 2500 volts set by the insulation of the electron gun; however, few measurements were made above 1000 volts, since no new features were found at higher voltages. The sizes of the retarding potential increments applied to the collector were dictated by the smallest currents which could be read with the desired accuracy. The applied potentials were 0, 5, 10, 20, 40, 90 volts. Smaller intervals would have been very desirable, particularly in the range below 10 volts where the refraction correction changes rapidly with

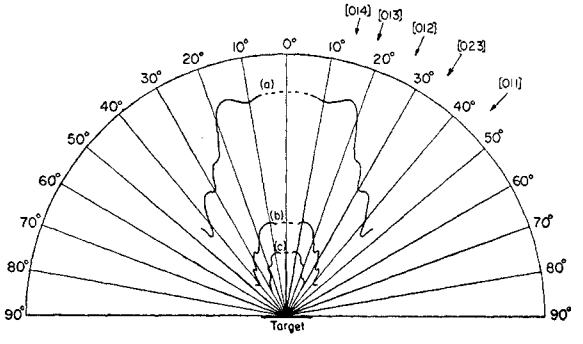

FIG. 8. Copper crystal, (001) face, 800-volt primary beam, normal incidence. Curve (a) is for 0–10 ev secondaries, index of refraction 1.29. Curve (b) is for 10–20 ev secondaries, index of refraction 1.36. Curve (c) is for 20–40 ev secondaries, index of refraction 1.48.

secondary electron energy, but the signal-to-noise ratio was such that smaller intervals were not practical in this experiment.

IV. RESULTS AND DISCUSSION

Before the measured angular distribution of secondary electrons can be analyzed in terms of the picture outlined above it is necessary to transform it into the shape that it has inside the metal before it is spread and distorted by refraction at the surface potential barrier. This is done by applying successively the solid angle and the refraction corrections as described previously. Figure 5 (solid curve) shows the external measured angular distribution from the (001) face of copper for secondaries in the energy range 0–10 ev and a primary electron energy of 250 ev. The dashed curve shows how the angular distribution appears after the solid angle correction $d\Omega'/d\Omega$ has been made, and the remaining curve shows the internal angular distribution obtained

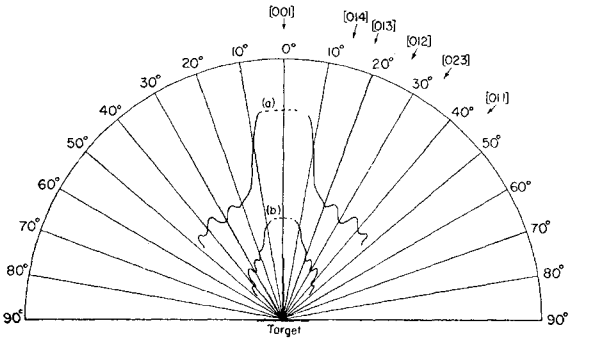

FIG. 9. Nickel crystal, (001) face, 250-volt primary electron beam, normal incidence. Curve (a) is for 0–10 ev secondaries; index of refraction 1.36. Curve (b) is for 10–20 ev secondaries; index of refraction 1.48.

by applying the refraction correction (Snell's law) to the dashed curve.

This procedure applied to the data of this experiment gives the angular distributions shown in Figs. 6–13. The refractive index was adjusted to put the prominent [012], [023], and [011] peaks in their proper positions for each energy group of secondaries. The index chosen in this way for electrons in a given energy range was found to be independent of primary energy and angle of incidence, as it should be. As mentioned earlier, in general one would expect that the index of refraction would vary somewhat with the direction of $\mathbf{k}'$; however, it is doubtful whether the precision of this experiment was adequate to detect this effect which would show itself in the form of shifts in the angular distribution peaks from their proper positions. Such shifts as were observed were within the estimated angular accuracy of the apparatus (~±3°).

Table I gives the refractive indices that were used to obtain the internal angular distributions shown in Figs. 6–13. The uncertainties in the values in this table are about ±3% and the differences in refractive index for the various energy groups of secondaries are well

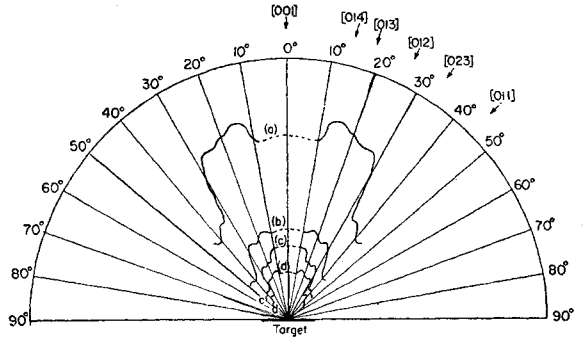

FIG. 10. Nickel crystal, (001) face, 500-volt primary electron beam, normal incidence. Curve (a) is for 10–20 ev secondaries, refractive index 1.36. Curve (b) is for 10–20 ev secondaries, refractive index 1.48. Curve (c) is for 20–40 ev secondaries, refractive index 1.30. Curve (d) is for 40–90 ev secondaries, refractive index 1.10.

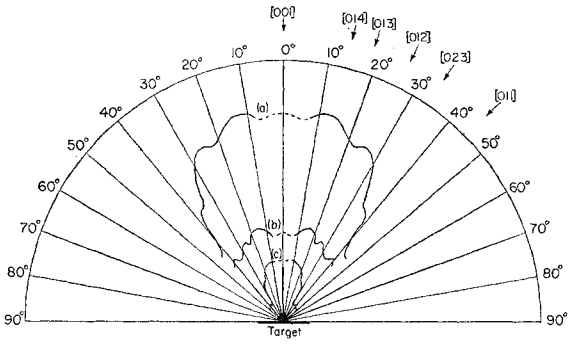

FIG. 11. Nickel crystal, (001) face, 800-volt primary electron beam, normal incidence. Curve (a) is for 0–10 ev secondaries, refractive index 1.36. Curve (b) is for 10–20 ev secondaries, refractive index 1.48. Curve (c) is for 20–40 ev secondaries, refractive index 1.30.

outside the estimated experimental uncertainty. In interpreting these indices it must be remembered that they are averages over relatively large energy increments weighted somewhat by the energy distribution of the secondaries. Table I also gives approximate values of the index according to the free electron model in which $\eta=(1+W/E_s)^{\frac{1}{2}}$ with $W\approx 12$ ev and rough, weighted average values of $E_s=4$, 13, 28, and 60 ev respectively for the four energy groups of secondaries. Only the refractive index of the most energetic group of secondaries (40–90 ev) agrees with the free-electron value. The departure from the free electron value is quite pronounced for the low energy secondaries.

Figures 6–8 show the angular distributions of internal secondaries in three energy groups (0–10 ev, 10–20 ev, and 20-40 ev) for a copper crystal with the primary electron beam normally incident on the (001) face. Each of these figures is for one of the primary electron energies used (250, 500, 800 electron volts). Figures 9–11 give the corresponding internal angular distributions for a nickel crystal with the primary beam striking the (001) face at normal incidence. The curves are extended as close to the critical angle for total internal reflection as the external observations warrant. (The measurements are

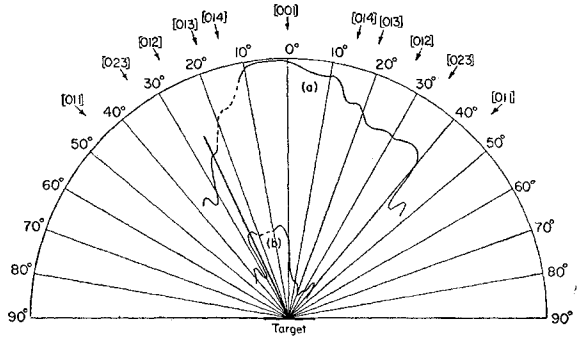

FIG. 12. Nickel crystal, (001) face, 500-volt primary beam incident at 25° from normal in the (001) plane. Curve (a) is for 0–10 ev secondaries; index of refraction 1.36. Curve (b) is for 10–20 ev secondaries; index of refraction 1.48.

reliable generally to 70–75% from the normal.) Although there are variations in the relative strengths of the various peaks in the different energy groups and in the same energy group at different primary energies, the main features of all these curves are similar. They all exhibit a broad central peak which according to our interpretation consists of secondaries scattered inelastically along the [001] direction and superimposed on this central peak appear smaller maxima in the [015], [014], [013] directions, rather poorly resolved in most cases. The peaks along the [012] and [023] directions generally appear well-defined, and there is frequently evidence of a peak at [011]. However, this latter peak is so strongly refracted at the surface of the crystal that it is emitted at angles of from 65° to 75° from the normal, depending on the refractive index, and the observations at such large angles of emission become increasingly difficult so it is not always possible in the data taken at normal incidence to observe the complete peak at 45° ([011] direction) but only one side of it. Qualitatively,

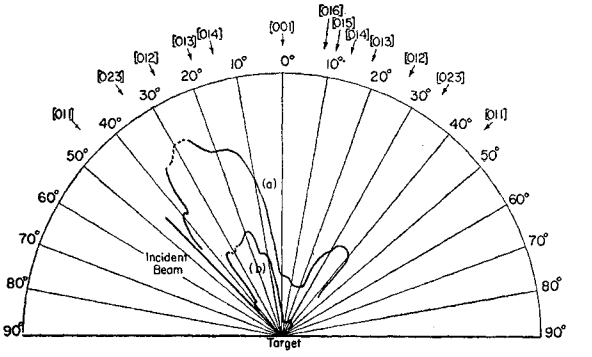

FIG. 13. Nickel crystal, (001) face, 800-volt primary electrons incident at 45° from the normal in the (100) plane. Curve (a) is for 0–10 ev secondaries; index of refraction 1.36. Curve (b) is for 10–20 ev secondaries; index of refraction 1.48.

these curves show clear evidence of maxima in the angular distributions in agreement with the theory, and the widths of these peaks insofar as one can determine them, diluted as they are by the large number of multiply scattered secondaries, are consistent with the predictions of theory.

The shape of the central peak could not be measured accurately for normal incidence because the electron collector intercepted the primary beam within approximately 8° on either side of the axis. However, some information about the shape of this peak was obtained by rotating the crystal about the [010] axis to give an angle of incidence θ_i. Figures 12 and 13 show the resulting internal angular distribution for primary beams incident at 25° and 45° from the normal respectively. Aside from the asymmetry which accompanies off-normal incidence, all the prominent peaks seen in Figs. 6–11 are present here also. This seems to be strong evidence that the observed peaks are actually properties of the crystals and not some accidental disposition of

contact potentials within the apparatus which by coincidence gives the observed structure to the angular distribution. The asymmetry which appears in the curves for non-normal primary incidence becomes more and more pronounced as the angle of incidence is increased. However, no satisfactory explanation for the cause of the asymmetry has yet been found. In Fig. 13 a definite peak appears at 40° on the side of the incident beam (incidence angle=45° in this figure). It is not certain whether this is a misplaced 45° [011] peak or not. The displacement of the peak in this case is greater than the experimental uncertainty if it is indeed the [001] peak.

Before the observed angular distribution peaks can be explained in terms of umklapp excitations according to the theory discussed earlier, it is necessary to rule out diffraction of the internal secondaries by Bragg planes in the crystal and by the surface lattice as possible origins of the angular structure. There are two kinds of evidence against diffraction as an explanation of the experimental results. First, the measured peaks are too narrow to be diffraction maxima, and second, they are too intense. To visualize the internal diffraction, consider the secondaries to be emitted at all angles from a localized source within the crystal. Those moving with appropriate energies and directions will be diffracted by various Bragg planes in the lattice according to the familiar Bragg equation. Each group of secondaries observed encompasses a relatively wide range of energies, and there is a correspondingly wide range of wavelengths for the internal secondaries. Consequently, the aggregate of the Bragg reflections from a given set of planes is spread over a wide and easily calculable angular interval. Comparison of the calculated angular spreads of the diffracted secondaries with the widths of the observed peaks shows the diffraction peaks to be much broader in all cases for the lower energy groups of emitted electrons. A similar statement can be made about diffraction by the two-dimensional surface lattice. In regard to intensity, if the internal secondaries move isotropically a rough upper limit on the intensity of the diffraction peaks can be determined by a simple geometrical calculation, and this upper limit turns out to be at least an order of magnitude too small to account for the experimental results. Consequently, there can be little doubt that diffraction plays a negligible role in the phenomena being considered here.

TABLE I. Experimental values of the index of refraction for various energy groups of secondary electrons from Cu and Ni determined from the angular distributions, together with approximate free-electron refractive indices in these metals.

Secondary energies	0–10 ev	10–20 ev	20–40 ev	40–90 ev
Copper	1.29	1.36	1.48	···
Nickel	1.36	1.48	1.30	1.10
Free electron	2.00	1.39	1.19	1.10

CONCLUSIONS

The most immediately evident result of the present work is that the angular distribution from single crystals of copper and nickel is not a simple cosine distribution as earlier work leads one to expect, but instead it possesses a considerable amount of structure in the form of weak maxima superimposed upon a background which has approximately a cosine distribution.

The observed structure in the angular distribution cannot be accounted for in terms of diffraction of the internal secondaries either by Bragg planes in the crystal or by the surface lattice. Instead, the observed angular distribution is found to be consistent with quantum-mechanical collision theories in which the role of the crystal lattice in conserving momentum is properly taken into account. The correct interaction potential to employ in such a collision theory is a screened Coulomb interaction with a velocity-dependent screening length giving weak screening at large velocities and strong screening at low velocities.

The explanation of the angular peaks in terms of such a collision theory presumes that an appreciable fraction of the internal secondaries, initially oriented more or less strongly along the principle crystal axes in accordance with momentum conservation requirements, can move to the surface of the crystal without suffering collisions that disturb the initial directions of motion. The implication is that the mean free paths of the secondaries are roughly comparable to those of the primaries. Although the prevailing view is that the secondaries have much shorter mean free paths than the primaries, this view is supported experimentally at present only by diffusion lengths which are adjusted to bring agreement between theoretical and measured total yield curves for polycrystalline samples and in these values may reside the accumulated errors introduced by the approximations made throughout the theory. The existence of comparable mean free paths for primaries and secondaries is qualitatively consistent with a screened interaction having a variable screening length. In such a case the slow secondaries are much more strongly screened than the primaries. As a result, the secondaries can undergo collisions with a much smaller number of lattice electrons (essentially only near neighbors) than the lightly screened primary. This restriction of the interaction distance for the secondaries decreases the collision rate markedly; on the other hand, the collision probability is inversely proportional to the energy of the incident particle in the collision [Eq. (1)], and this factor increases the collision probability for the slow secondaries compared with that of the primaries. It is conceivable that these opposing influences could counteract each other, resulting in a mean free path for the secondaries roughly comparable to that of the primaries. Certainly the present results imply that this is the case.

In order to interpret the observed angular distribu-

tion, it is necessary to correct for refraction at the surface of the crystal to obtain a picture of the internal distribution of the secondaries. This correction involves the choice of a refractive index for the crystal. For each crystal studied it was possible to find by trial a unique value of the refractive index for each energy group of secondaries which gave consistent internal angular distributions for all primary energies and angles of incidence employed. The distribution so obtained gave peaks whose positions and widths are in agreement with the theory for interzone transitions. The values of the refractive indices obtained in this manner differ markedly from free-electron refractive indices in the range of low and medium secondary energies. The implication is plainly that electrons of these energies in nickel and copper are not free, or nearly free,[12] and with refinement the study of angular distributions may be used as a tool to study in detail departures from the free electron approximation in the excited states of many solids. Since the refractive index is proportional to $\nabla_k E(\mathbf{k})$, it is possible in principle to determine the shape of the $E(\mathbf{k})$ curve for these excited states, given sufficiently detailed information about the index of refraction.

V. ACKNOWLEDGMENTS

The author is pleased to thank Professor Robert Gomer, Professor Andrew Lawson, and Professor Morrel Cohen of the Institute for Study of Metals and Dr. Foster Rieke of Chicago Midway Laboratories for many helpful discussions and suggestions during the course of this work. Thanks is also due Mr. Paul Dolon and Mr. Paul Husted for their help in fabricating parts of the apparatus.

PHYSICAL REVIEW VOLUME 119, NUMBER 1 JULY 1, 1960

Temperature Dependence of Optical Bleaching of KCl Crystals near 0°C*

W. E. BRON AND A. S. NOWICK
International Business Machines Research Center, Yorktown Heights, New York
(Received February 12, 1960)

Further insight has been sought into the mechanism of optical bleaching in the vicinity of room temperature by studying the temperature dependence of the bleaching curves for KCl crystals which had been initially irradiated with hard (filtered) x-rays. The absorptions at the maxima of the F, M, R_1, and R_2 bands were observed to change during illumination with F-light and to be strongly temperature dependent in the range of -30°C to $+10$°C, whereas the absorption at the V_3 band was essentially unchanged. For comparison an analysis was made of the data of Petroff on the early growth of the M band during bleaching with F-light in additively colored KCl crystals. In this case a unique activation energy, ϵ, of 0.35 ± 0.05 ev and a number of defect jumps $N_j \approx 10^{10}$ are indicated by the data. It appears that the bleaching curves of the x-irradiated samples are composed of a temperature independent and a temperature dependent part. The temperature dependent part probably is the same as that responsible for bleaching in additively colored crystals. The above results for ϵ and N_j suggest that the temperature dependent bleaching process results from the trapping of photoelectrons at vacancy clusters which are formed during bleaching through the migration of mobile defects, possibly vacancy pairs. This conclusion is supported by the observations by others that the α band is not observed during bleaching at room temperature.

INTRODUCTION

A NUMBER of mechanisms have been proposed to account for experimental results obtained when F centers in alkali halides are bleached with light in the F band in the vicinity of room temperature. Among the mechanisms proposed are the following: Bleaching occurs when (i) the photoelectrons produced through the ionization of F centers are annihilated at holes associated with V centers[1–3] (ii) photoelectrons are captured by clusters of vacancies, which results in the production of secondary color centers either immediately or after a suitable ejection of surplus vacancies from the cluster,[4] and (iii) negative-ion vacancies obtained through the ionization of F centers combine with other vacancies and migrate to form aggregates, which upon the proper acquisition of photoelectrons form R, M, and N centers.[5] The bleaching of F centers through the formation of F' centers need not be considered as a possible mechanism, since in alkali halides such as NaCl and KCl the F' center is not stable in the vicinity of room temperature.[6]

It will be convenient to refer to the bleaching mechanisms which involve diffusion of defects as "defect-migration" mechanisms, and to refer to the mechanisms which involve only the motion of electrons from F centers to existing electron trapping centers as "elec-

* Part of a thesis submitted by W. E. Bron in partial fulfillment of the requirements for the degree of Doctor of Philosophy in the Faculty of Pure Science, Columbia University, 1959. This paper was originally presented at the International Symposium on Color Centers in Alkali Halides, at Oregon State College, September, 1959.

[1] E. E. Schneider, *Photographic Sensitivity* (Butterworths Scientific Publications, London, 1951), p. 13.

[2] I. L. Mador, R. F. Wallis, M. C. Williams, and R. C. Herman, Phys. Rev. **96**, 617 (1954).

[3] F. Seitz, Revs. Modern Phys. **26**, 7 (1954).

[4] M. Ueta and W. Känzig, Phys. Rev. **97**, 1591 (1955).

[5] F. Seitz, Revs. Modern Phys. **18**, 384 (1946).

[6] H. Pick, Ann. Physick **31**, 365 (1938).